International Journal of Biological Macromolecules 304 (2025) 140751

Contents lists available at ScienceDirect

International Journal of Biological Macromolecules

journal homepage: www.elsevier.com/locate/ijbiomac

Near-infrared light-triggered nitric oxide-releasing hyaluronic acid hydrogel for precision transdermal therapy of androgenic alopecia

Hui Xing [a,b,1], Yucheng Wang [a,b,1], Shengling Huang [c,1], Huanqi Peng [a,b], Ziyi Zhao [a,b], Yuhui Yang [a,b], Xiaoxu Zhu [a,*], Guowei Li [d,*], Dong Ma [a,b,**]

[a] Department of Burn and Plastic Surgery, Guangzhou Red Cross Hospital, Jinan University, Guangzhou 510235, China
[b] MOE Key Laboratory of Tumor Molecular Biology, Key Laboratory of Biomaterials of Guangdong Higher Education Institutes, Department of Biomedical Engineering, Jinan University, Guangzhou 510632, China
[c] Department of Nephrology, The First Affiliated Hospital of Jinan University, Guangzhou 510630, China
[d] Department of Nuclear Medicine and PET/CT-MRI Center, The First Affiliated Hospital of Jinan University, Jinan University, Guangzhou 510630, China

ARTICLE INFO

Keywords:
Androgenetic alopecia
Nitric oxide
Hyaluronic acid hydrogel

ABSTRACT

Progressive follicle and vascular atrophy, insufficient nutrient supply, and hormonal imbalance are direct causes of androgenic alopecia (AGA), limiting treatment options. Nitric oxide (NO) has demonstrated significant advantages in cell proliferation, vascular repair, and inflammation regulation. However, precise control of NO concentration and efficient utilization limit its clinical application for AGA treatment. To address this, we developed a near-infrared (NIR) light-triggered NO-releasing delivery system (Gel@L-Arg). The system uses Chlorin e6 (Ce6) grafted onto oxidized hyaluronic acid, reacting with L-Arg-loaded polyethyleneimine *via* Schiff base to form hyaluronic acid hydrogel. Under NIR light, Ce6 generates ROS, oxidizing L-Arg to release NO, after 5 min of irradiation, the NO concentration in Gel@L-Arg (1 %) is >1.5 times that in Gel@L-Arg (0.5 %), enabling on-demand release of NO. Gel@L-Arg (0.5 %) effectively promotes angiogenesis while significantly repairing damaged human dermal papilla cells (HDPCs), with cell viability reaching 131.6 ± 4.6 %. In animal models, the system reduced inflammation (IL-6, TNF-α), enhanced nutrient supply (VEGF, CD31), regulated androgens, and improved the follicular microenvironment, effectively treating AGA. This hyaluronic acid hydrogel, combining NIR light-triggered release with gas therapy, offers a new strategy for the treatment of AGA with good biocompatibility, providing insight into controlled gas release therapies for disease treatment.

1. Introduction

As the most common type of clinical hair loss worldwide, androgenetic alopecia (AGA) poses a significant threat to patients' physical and mental health [1]. Its complex pathogenesis includes progressive follicle and vascular atrophy, nutrient deficiency, hormonal imbalance, and genetic factors, all of which make treatment particularly challenging [2]. Currently, the only FDA-approved drugs for AGA are Minoxidil and Finasteride, however, both are associated with significant side effects, including dermatitis, hypertrichosis, and testicular pain, particularly with long-term use [3]. Despite advances in medical technology and the development of alternative therapies such as phototherapy, hormone therapy, injections, and hair transplantation, these options are expensive, complex to administer, and often fail to provide lasting benefits [4]. Therefore, it is crucial to develop a safe and effective therapy that targets the underlying pathogenesis of AGA.

Our team has long been dedicated to studying the functions of nitric oxide (NO), an endogenous diatomic gas molecule that plays a crucial role as a signaling mediator in various physiological and pathological processes, including vasodilation, cell migration, and immune responses [5,6]. Research indicates that the effects of NO are highly dependent on its concentration. High concentrations of NO can induce cytotoxic effects through mechanisms such as mitochondrial damage, DNA damage, and inhibition of cellular respiration, whereas low concentrations of NO

* Corresponding authors.
** Correspondence to: Dong Ma, MOE Key Laboratory of Tumor Molecular Biology, Key Laboratory of Biomaterials of Guangdong Higher Education Institutes, Department of Biomedical Engineering, Jinan University, Guangzhou 510632, China.
E-mail addresses: zhuxx35@mail.sysu.edu.cn (X. Zhu), liguowei@jnu.edu.cn (G. Li), tmadong@jnu.edu.cn (D. Ma).
[1] H.X., Y·W and S.H. contributed equally to this work.

https://doi.org/10.1016/j.ijbiomac.2025.140751
Received 22 November 2024; Received in revised form 18 January 2025; Accepted 5 February 2025
Available online 6 February 2025

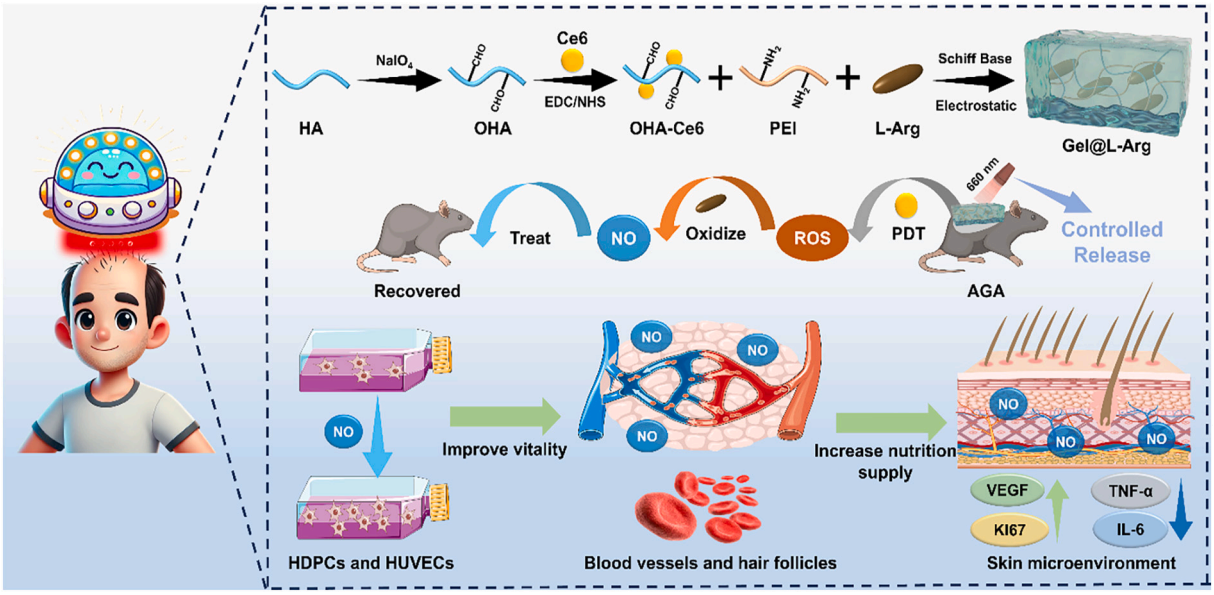

Scheme 1. Schematic illustration of the NIR light-triggered NO-releasing hyaluronic acid hydrogel transdermal delivery system for treating AGA.

demonstrate beneficial reparative functions, including immune modulation, enhanced cell viability, promotion of cell migration, and angiogenesis [7]. Therefore, low-concentration NO has the potential to treat AGA by restoring follicular cells, suppressing inflammation, and dilating blood vessels to improve follicular nutrient supply. However, the short half-life of NO, its non-specific distribution, difficulties in controlled release, and challenges in regulating its concentration significantly limit its further clinical application [8]. Consequently, the therapeutic use of NO in AGA relies on developing controlled and adjustable NO release, ideally in a patient-manageable format.

L-arginine (L-Arg), a natural NO donor with high biocompatibility, can produce NO through ROS catalysis. However, endogenous ROS levels in skin and follicle cells are insufficient to generate adequate NO [9]. Recently, Shi et al. designed a nanoparticle (EArgFe@Ce6), wherein near-infrared (NIR) irradiation enables Chlorin e6 (Ce6) within the nanoparticles to produce ROS that catalyzes L-Arg into NO. Ce6, a widely used photosensitizer with a maximum absorption wavelength of 660 nm, low-level laser therapy (LLLT), an FDA-approved method, has demonstrated certain effectiveness in treating AGA. Building on previous research on light-controlled release technology [10], we were inspired to explore the potential of mimicking the effects of LLLT. This approach aims to address the controlled release of NO using NIR light and regulate the concentration of L-Arg to effectively release NO. The transdermal delivery system, praised for its non-invasive nature, avoidance of the first-pass effect, and high efficiency, is considered one of the most promising non-invasive drug delivery methods. However, the stratum corneum, as the skin's primary protective layer, presents a significant barrier due to its semi-permeable membrane-like properties, making it difficult to permeate. In recent years, hydrogel-based transdermal patches have been extensively applied in drug delivery. The porous structure of semi-solid hydrogels enables the loading of drugs or cells and their adhesion to human skin, facilitating sustained transdermal delivery with high safety [11]. For instance, Zheng et al. developed a tissue-adhesive hydrogel based on the synergistic effect of cohesion and adhesion, which demonstrated a 4.9-fold increase in adhesive strength compared to control patches and potential for transdermal drug delivery as proven by *in vitro* studies [12]. By simulating LLLT, the hydrogel as a carrier provides a potential solution for the controlled release of NO using NIR light. It also allows for the effective transdermal delivery of NO by adjusting the concentration of L-Arg, offering a feasible approach for skin applications and facilitating patient self-management.

In this study, to address challenges such as uncontrolled NO release and concentration regulation, we drew on the clinical experience of LLLT and integrated NIR light-triggered release technology, hydrogel-based transdermal delivery, and the therapeutic potential of NO for AGA treatment. Activated OHA was reacted with Ce6 to form a photo-responsive trigger (OHA—Ce6) *via* amide bonds. This was then combined with a PEI solution loaded with the NO donor L-Arg (PEI@L-Arg) through Schiff base reactions and electrostatic reaction to create the NIR light-triggered NO-releasing hydrogel system (Gel@L-Arg) (as shown in Scheme 1). First, we characterized the preparation process of Gel@L-Arg and explored the NIR light-triggered NO release effect by adjusting L-Arg concentration. Subsequently, we conducted *in vitro* experiments to investigate the effects of NO on enhancing cell viability and modulating inflammation in human dermal papilla cells (HDPCs) damaged by dihydrotestosterone (DHT), as well as the potential of low-concentration NO for vascular repair and improving follicle nutrient supply. Finally, we established an AGA mouse model and evaluated the *in vivo* therapeutic effects of the hydrogel system using various indicators, revealing the underlying mechanism of NO in AGA treatment. Therefore, we innovatively achieved concentration modulation of NO through a NIR controlled release system for efficient transdermal treatment of AGA, meeting the personalized treatment needs of patients. By combining light-controlled release systems with gas therapy, we have provided a new approach for treating AGA and offered new insights for the combined treatment of skin-related diseases.

2. Materials and methods

2.1. Materials preparation

Sodium hyaluronate (Mn = 250 k) and Chlorin e6 were purchased from Yuanye Bio-Technology Co., Ltd. (Shanghai, China). Sodium periodate was obtained from Boyle Chemical Reagents (Shanghai, China). L-arginine (L-Arg) and polyethyleneimine (PEI, Mn = 10 k) were purchased from Sigma. Minoxidil tincture was purchased from Dafeixin. Griess reagent kit, CCK-8 assay, and SOSG singlet oxygen probe were purchased from Beyotime Biotechnology Co., Ltd. (Shanghai, China). Human dermal papilla cells (HDPCs) were obtained from Meisen Cell Technology Co., Ltd. (Zhejiang, China). Human umbilical vein endothelial cells (HUVECs) were obtained from Procell Life

Science&Technology Co., Ltd. (Wuhan, China).

2.2. Synthesis and characterization of Gel@L-Arg

2.2.1. Synthesis of OHA

Oxidized hyaluronic acid (OHA) was synthesized by reacting hyaluronic acid (HA) with $NaIO_4$, following a previously reported method with modifications [13,14]. Briefly, 2.5 g of HA was dissolved in 100 mL of deionized water and stirred until fully dissolved. Then, 1.0 g of $NaIO_4$ was added, and the reaction was stirred at room temperature in the dark for 24 h. Afterward, 100 μL of glycerol was added to terminate the reaction, with an additional 1 h of stirring. The product was then placed in a 10 kDa dialysis bag and dialyzed against deionized water for 72 h. Finally, the product was freeze-dried to obtain a white solid of OHA.

2.2.2. Synthesis of OHA-Ce6

The synthesis of OHA-Ce6 was conducted following previously reported procedures with slight modifications [15]. Initially, 0.2 g of OHA, 16.7 mg of EDC, and 12.1 mg of NHS were dissolved in 18 mL of PBS(pH = 7.4). In a separate preparation, 0.2 g of ethylenediamine (EDA) was dissolved in 2 mL of PBS and subsequently combined with the initial solution. The reaction mixture was stirred at room temperature in the dark for 12 h. The resultant product was transferred to a 1 kDa dialysis bag and dialyzed against deionized water for 48 h. Following this, 5 mL of the dialysate was mixed with 5 mL of DMSO, to which 2 mg of Ce6, 1.6 mg of EDC, and 1.32 mg of NHS dissolved in 10 mL of DMSO were added. This mixture was stirred at room temperature in the dark for 24 h and subsequently dialyzed in a 1 kDa dialysis bag against deionized water for another 48 h. The final product was freeze-dried, yielding a yellow powder form of OHA—Ce6.

2.2.3. Synthesis of Gel@L-Arg

The synthesis of Gel@L-Arg was achieved *via* a Schiff base reaction between the active aldehyde groups of OHA and the amino groups in PEI, along with electrostatic interactions [16]. First, 0.1 g of PEI was dissolved in 10 mL of PBS to obtain a 1 % PEI solution. Then, 0.2 g or 0.1 g of L-Arg was added, yielding PEI@L-Arg solutions with L-Arg concentrations of 1 % and 0.5 %, respectively. Separately, 3 g of OHA-Ce6 was dissolved in 10 mL of PBS to create a 30 % OHA-Ce6 solution. Equal volumes of the PEI@L-Arg and OHA-Ce6 solutions were mixed at a 1:1 ratio and gently shaken for 30 s to form Gel@L-Arg with different L-Arg concentrations.

2.2.4. Characterization

HA and OHA were dissolved in deuterium oxide, and their ^1H NMR spectra were recorded using a Bruker 300 NMR spectrometer. Fourier-transform infrared spectroscopy (FTIR) (VERTEX70) with potassium bromide (KBr) pellet method was used to assess structural changes between HA and OHA. A UV spectrophotometer (UV-2550) was used to measure spectral changes in Ce6, OHA, and OHA—Ce6. The surface morphology of the freeze-dried hydrogel was observed using a scanning electron microscope (SEM) operated at 20 kV. A rotational rheometer was used to analyze the hydrogel's rheological properties, with a time sweep range of 0–300 s and a temperature sweep range of 10–40 °C, both at 1 % strain and 1 Hz frequency.

2.3. NIR light-triggered NO release performance in Gel@L-Arg

2.3.1. ROS release evaluation

The singlet oxygen ($^1O_2$) content after light irradiation of the material was measured using SOSG as a fluorescent probe [17]. 2.5 μL of a 100 μM SOSG solution was added to 97.5 μL of OHA-Ce6@L-Arg. After irradiating with a 660 nm laser for 1, 3, and 5 min, the fluorescence intensity of the solution was measured using a multifunctional microplate reader. The control group consisted of OHA-Ce6 solution with the SOSG probe but without light irradiation.

2.3.2. In vitro NO release test

The NO release from the hydrogel was assessed using the Griess reagent. Each sample of Gel@L-Arg (0.5 %) and Gel@L-Arg (1 %) (100 μL) was mixed with 100 μL PBS and irradiated with a 660 nm laser for 1, 3, and 5 min. After each irradiation period, fresh PBS was added, and the solution was centrifuged. A 100 μL aliquot of the supernatant was mixed with 100 μL of Griess reagent, and the absorbance at 540 nm was measured using a multifunctional microplate reader [18]. The NO release amount was determined from a standard curve based on absorbance, and a NO release curve was plotted for different arginine concentrations.

2.4. Cell experiments

2.4.1. Cell proliferation

Human umbilical vein endothelial cells (HUVECs) were seeded at a density of 5×10^3 cells/well in 96-well plates and incubated at 37 °C in a 5 % CO_2 environment for 24 h. The medium was then replaced with complete medium containing Minoxidil (0.02 %), Gel@L-Arg (0.5 %), or Gel@L-Arg (1 %), with DHT (0.02 %) added to all media except the control group. After 24 h, the materials were removed, and CCK-8 reagent was added. Absorbance was measured at 450 nm using a multifunctional microplate reader [6], and cell proliferation rates were calculated. The human dermal papilla cells (HDPCs) proliferation experiment was performed similarly.

2.4.2. Cell migration

The scratch assay was used to assess the effect of materials on cell migration [19]. Briefly, HUVECs were seeded at 2×10^5 cells/well in 6-well plates. When cell confluence reached 80 %–90 %, a scratch was made using a 200 μL pipette tip. After washing twice, the medium was replaced with complete medium containing Minoxidil (0.02 %), Gel@L-Arg (0.5 %), or Gel@L-Arg (1 %), with DHT (0.02 %) added to all media except the control. After 24 h, cell migration was observed and scratch width was measured with ImageJ software. The HDPCs migration experiment was performed similarly.

2.4.3. Angiogenesis

HUVECs were cultured in complete medium containing Minoxidil (0.02 %), Gel@L-Arg (0.5 %), or Gel@L-Arg (1 %) for 48 h, with DHT (0.02 %) added to all media except the control. For the assay, 200 μL of Matrigel was spread in a 12-well plate and incubated at 37 °C for 15 min to solidify. Treated cells were seeded at a density of 5×10^5 cells/well onto the polymerized Matrigel and incubated for 8 h. Tube formation was observed under a microscope, and the number of tubes was quantified using ImageJ software [20].

2.4.4. qRT-PCR analysis

qRT-PCR was performed to investigate the expression of genes related to Gel@L-Arg treatment in damaged HDPCs [21]. HDPCs were cultured in 6-well plates at a density of 2×10^5 cells/well. When cell confluence reached 80 %–90 %, the cells were washed and replaced with complete medium containing Minoxidil (0.02 %), Gel@L-Arg (0.5 %), or Gel@L-Arg (1 %), with DHT (0.02 %) added to all media except the control. After 24 h, RNA was extracted, and reverse transcription was performed following the kit instructions. qRT-PCR was then used to detect IL-6 and MMP9 expression. Primer sequences are listed in Table S1.

2.5. Animal experiments

2.5.1. AGA model establishment

The model was established as previously described [22]. In choosing the gender of the mice, in addition to excluding the impact of male hormones on the establishment of the AGA model, we also considered that there is relatively less research on female AGA, and the number of

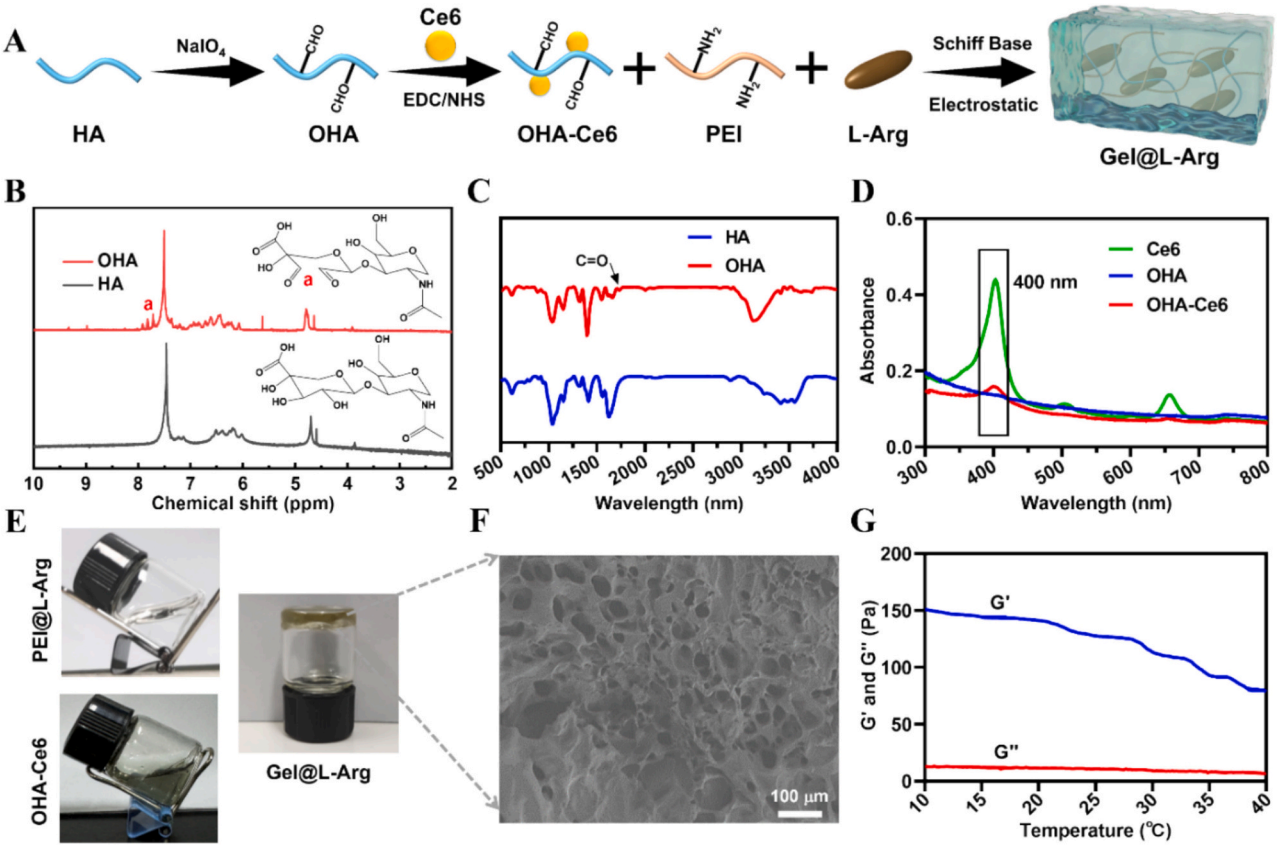

Fig. 1. Synthesis and characterization of Gel@L-Arg. (A) Schematic diagram of the synthesis of Gel@L-Arg. (B) ^{1}H NMR spectra of OHA and HA. (C) FTIR spectra of OHA and HA. (D) UV–Vis spectra of OHA—Ce6, Ce6, and HA. (E) Gelation effect of Gel@L-Arg. (F) SEM image of Gel@Arg. (G) Temperature stability test of Gel@L-Arg.

female patients with AGA is gradually increasing, which may have severe psychological impacts. Female C57BL/6 mice were acclimatized for one week at Jinan University Animal Facility. Animal handling complied with the Guidelines for the Care and Use of Laboratory Animals (2011) and Jinan University Animal Ethics Committee requirements (Approval No. IACUC-20240709-04). After acclimation, 24 mice were randomized into six groups (Healthy, AGA, Gel@L-Arg (0.5 %), Gel@L-Arg (0.5 % + NIR), Gel@L-Arg (1 % + NIR), and Minoxidil) with four mice per group and an average body weight of 20 g. Hair was removed using depilatory cream (Veet), and, except for the Healthy group, mice received daily subcutaneous injections of DHT (10 mg/kg/day) for 21 days to maintain androgen levels. Treatment was applied daily, and hair growth was tracked on days 7, 12, 17, and 21 with dermoscopy to observe skin changes.

2.5.2. Hair growth and histological evaluation

At the end of the experiment, newly grown hair on the mice's backs was carefully collected for microscopic observation and weighed. A 1 cm^2 skin section was excised, fixed in 4 % paraformaldehyde, embedded in paraffin, and sectioned for H&E staining, immunohistochemistry (CD31, Ki67, 3-nitro-tyrosine), and examination of hair follicles under a light microscope. The total hair follicle count was measured using ImageJ software [23].

2.5.3. Elisa

Skin tissue was homogenized in ice water to prepare a 10 % homogenate, centrifuged at 3000 rpm for 10 min, and the supernatant was collected for analysis. IL-6 and TNF-α were detected using a double-antibody sandwich ELISA, with color intensity proportional to concentration [24].

2.5.4. Mouse skin tissue immunofluorescence staining

Frozen skin sections from treated mice were subjected to immunofluorescence staining. After serum blocking, tissues were permeabilized, incubated with primary antibodies at 4 °C overnight, washed, and incubated with fluorescently labeled secondary antibodies.

2.6. Biocompatibility analysis

During treatment, dermoscopy was used to monitor sensitization of each group's dorsal skin. After 21 days, mice were euthanized, and major organs and serum were collected for safety evaluation. Blood was collected, centrifuged to obtain serum, and used for further biochemical analysis [25,26].

2.7. Statistical analysis

All data are presented as mean ± standard deviation. Differences between different experimental groups were analyzed using the One-way ANOVA method in GraphPad software (Inc., LA Jolla, CA, USA). The significance of differences was determined based on *P* values, where $^{*}P < 0.05$; $^{**}P < 0.01$; $^{***}P < 0.001$; $^{****}P < 0.0001$.

3. Results and discussions

3.1. Preparation and characterization of Gel@L-Arg

In this study, we successfully developed a near-infrared (NIR) light-triggered NO hydrogel delivery system. To confirm the successful synthesis of OHA within this hydrogel system, ^{1}H NMR spectroscopy was utilized to observe structural changes (Fig. 1B). The proton absorption

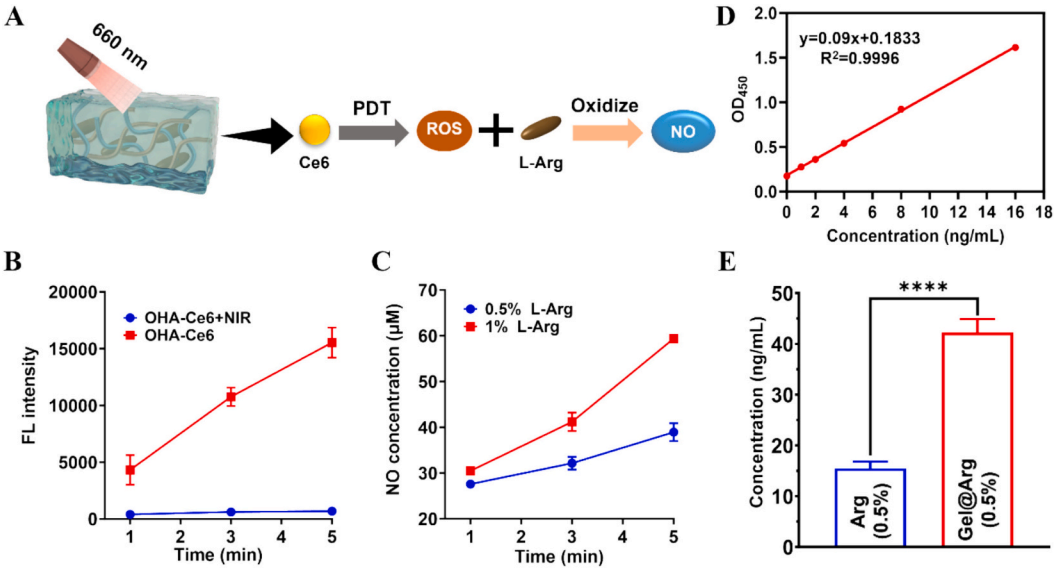

Fig. 2. Study on ROS and NO release from Gel@L-Arg. (A) Schematic diagram of NO generation. (B) ROS generation curve under 660 nm NIR irradiation ($n = 3$). (C) NO release curve of Gel@L-Arg (n = 3). (D) Standard curve of L-Arg at different concentrations (0, 1, 2, 4, 8, 16 ng/mL). (E) L-Arg (0.5 %) and Gel@Arg (0.5 %) *in vitro* permeation experiment showing the L-Arg content in the skin.

peak at position "a" corresponds to the aldehyde group of OHA. Additionally, FTIR characterization of OHA (Fig. 1C) demonstrated a characteristic absorption peak of the C═O group at 1730 cm^{-1}, further verifying the successful preparation of OHA [27]. To confirm the successful grafting of the photosensitizer Ce6 onto OHA, as illustrated in Fig. 1D, OHA-Ce6 exhibited a UV absorption peak around 400 nm,

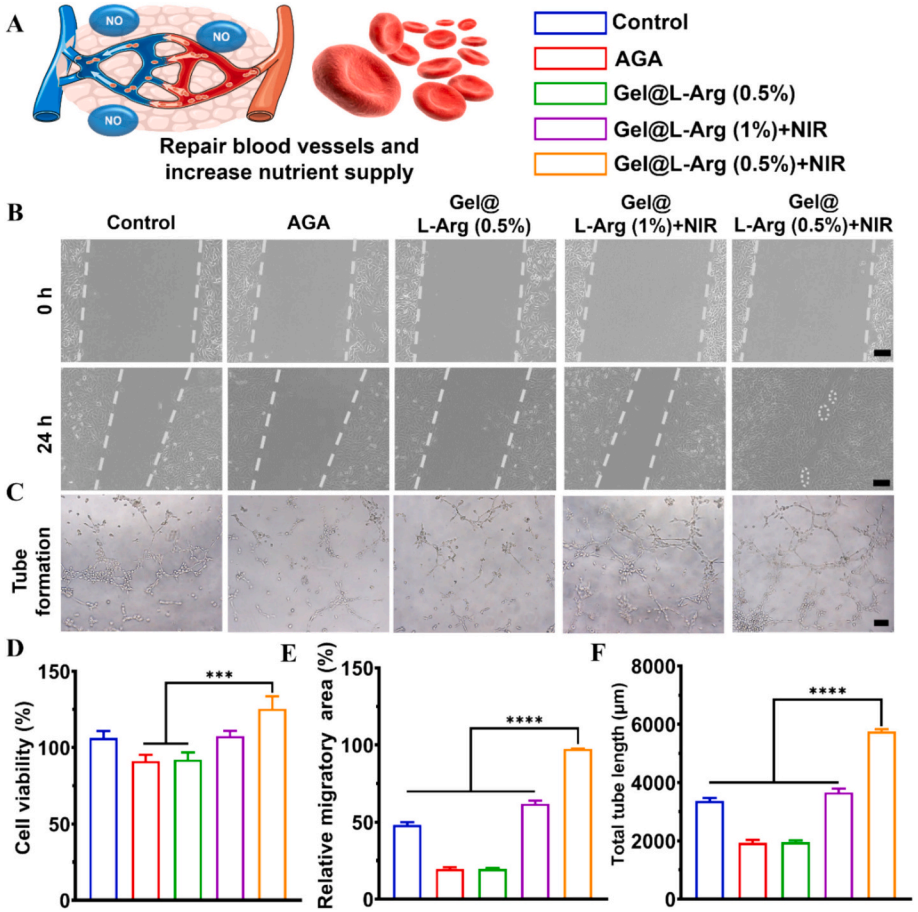

Fig. 3. Study on the promotion of vascular repair. (A) Schematic diagram of vascular generation promoted by Gel@L-Arg. (B) Migration images of HUVECs, scale bar = 100 μm. (C) Tube formation images of HUVECs, scale bar = 100 μm. (D) HUVECs proliferation ($n = 3$). (E) Quantitative analysis of relative migration area (n = 3). (F) Quantitative analysis of total tube length in HUVECs (n = 3). *$P < 0.05$; **$P < 0.01$; ***$P < 0.001$; ****$P < 0.0001$.

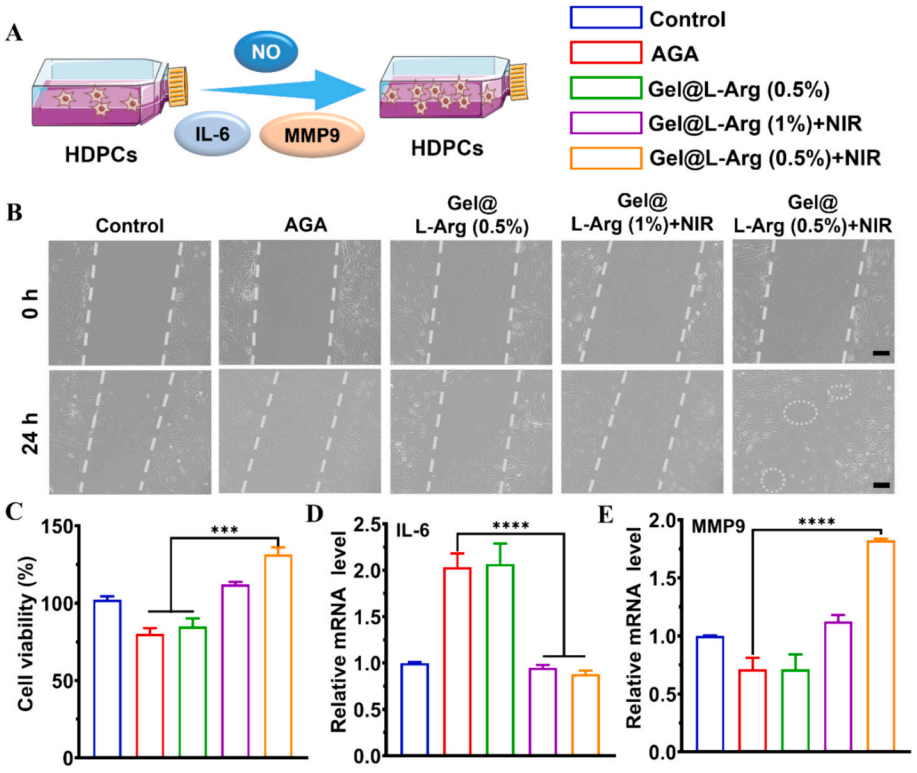

Fig. 4. Mechanistic study of Gel@L-Arg in repairing damaged hair follicles. (A) Schematic diagram of action of NO on HDPCs. (B) Migration images of HDPCs, scale bar = 100 μm. (C) HDPCs proliferation ($n = 3$). (D) mRNA levels of IL-6 in HDPCs (n = 3). (E) mRNA levels of MMP9 in HDPCs (n = 3). $^{*}P < 0.05$; $^{**}P < 0.01$; $^{***}P < 0.001$; $^{****}P < 0.0001$.

similar to that of Ce6, which was absent in OHA, indicating the successful synthesis of OHA-Ce6 [15]. Subsequently, varying amounts of L-Arg were dissolved in PEI to obtain PEI@L-Arg solutions with different concentrations, which were then mixed with the OHA-Ce6 solution at a 1:1 volume ratio to form the Gel@L-Arg. As shown in Fig. 1F, the freeze-dried hydrogel displayed a uniform three-dimensional porous structure, potentially enabling effective L-Arg loading for NO release. To meet practical clinical needs, a rheometer was used to assess both the time stability and temperature stability of the hydrogel. As shown in Fig. 1G, rheological scanning at different temperatures revealed that within the normal skin temperature range, the storage modulus (G') of the hydrogel was significantly higher than its loss modulus (G"), indicating stable hydrogel formation and temperature stability [28]. Furthermore, time stability testing of the hydrogel, as depicted in Fig. S1A, showed that it retained its gel state over clinically relevant treatment durations, effectively meeting the requirements for light irradiation. To better compare the characteristics of different hyaluronic acid hydrogels, we conducted a comprehensive literature review to identify similar hyaluronic acid hydrogels and their changes in G' and G" after 5 min of application to the skin at 37 °C. The results were summarized as shown in Fig. S1B. We found that in all the studies reviewed, G' was greater than G", which further indicates that the hyaluronic acid hydrogel used in this study remains stable at body temperature, meeting the requirements for skin application.

3.2. NIR light-triggered NO-releasing performance

Chlorin e6 (Ce6) is a commonly used photosensitizer with high efficiency in reactive oxygen species (ROS) generation under NIR light. However, its poor water solubility limits its application [29]. To enhance the water solubility of Ce6, we grafted it onto OHA and used a singlet oxygen fluorescent probe (SOSG) to detect its ROS generation capability under both light and dark conditions. As shown in Fig. 2B, OHA-Ce6 exhibited strong fluorescence intensity under 660 nm NIR irradiation, increasing with prolonged exposure, while negligible ROS generation was observed without irradiation. This result demonstrates that OHA-Ce6 exhibits effective NIR light-triggered ROS generation, providing a feasible approach for controlled NO release. To further verify the controlled release of NO, we explored the NO-release performance of Gel@L-Arg by varying the concentrations of L-Arg and the irradiation duration. As shown in Fig. 2C, the NO release curves indicated that with increased laser exposure time, NO levels produced by 1 % L-Arg rapidly rose, reaching 59.4 ± 0.7 μM. In contrast, NO release from 0.5 % L-Arg was slower, reaching 38.9 ± 2.0 μM. This demonstrates that the hydrogel allows for controlled NO release by adjusting L-Arg concentrations, enabling tunable NO delivery. To further validate the transdermal delivery capability of the gel, *in vitro* skin permeation experiments were conducted using a Franz diffusion cell with Arg (0.5 %) and Gel@Arg (0.5 %). As shown in Fig. 2D, E, after 3 h of *in vitro* permeation, the concentration of L-Arg in the skin was calculated based on the standard curve. The results showed that the presence of the gel effectively promoted the penetration and retention of L-Arg in the skin, achieving a concentration of 42.2 ± 2.6 ng/mL. This ensures the subsequent efficacy of L-Arg.

3.3. NO effectively promotes vascular repair

Studies have shown that vascular degeneration around hair follicles in AGA patients significantly impairs blood supply, leading to follicle miniaturization. Enhancing vascular repair and improving follicle nutrition is crucial for hair regeneration [30]. Therefore, this experiment investigated the effects of NO generated by Gel@L-Arg before and after irradiation on human umbilical vein endothelial cells (HUVECs) to evaluate its potential for vascular repair. Dihydrotestosterone (DHT) was used to simulate the androgenic environment in patients. Cell viability was reduced in the AGA group compared to the Control,

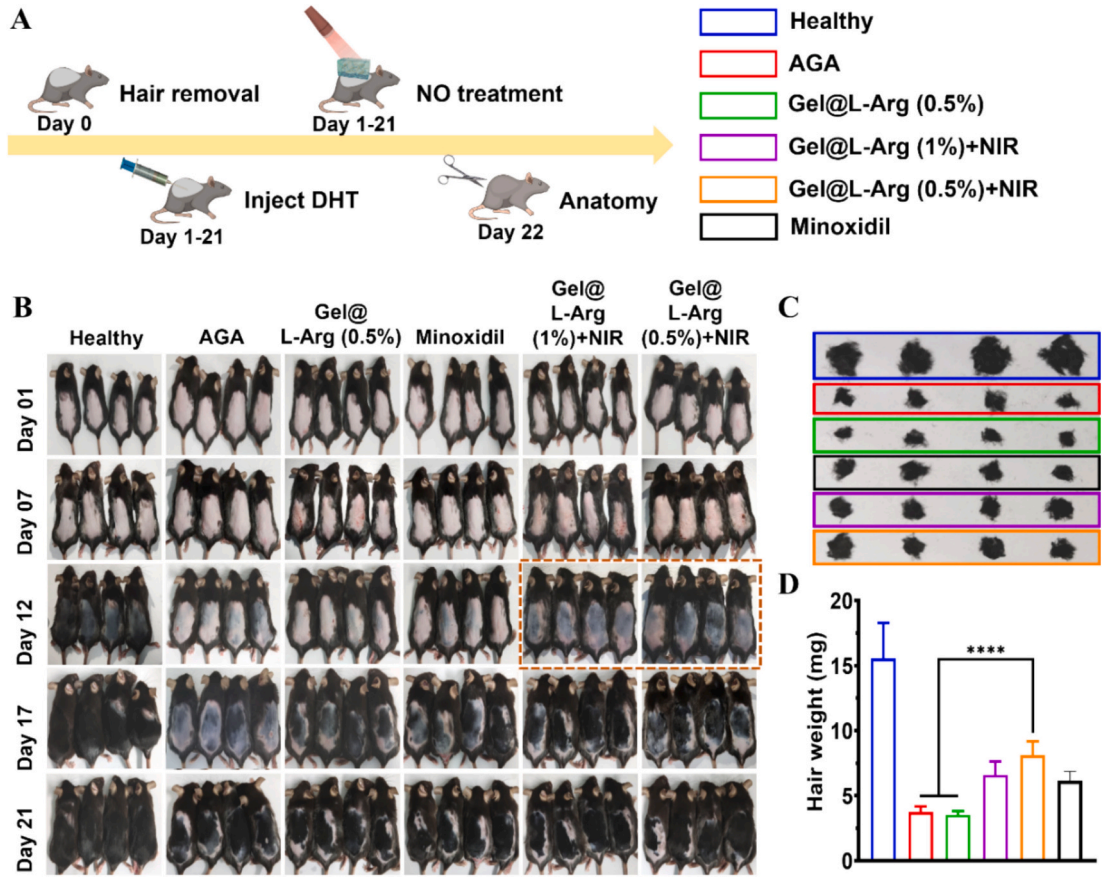

Fig. 5. Evaluation of hair regeneration. (A) Establishment and subsequent treatment of the AGA mice model. (B) Dorsal images of mice over the 21-day treatment period. (C) Overall picture of regrowing hair ($n = 4$). (D) Regenerated hair weight (n = 4). *$P < 0.05$; **$P < 0.01$; ***$P < 0.001$; ****$P < 0.0001$.

indicating that DHT exerted a negative effect on HUVECs proliferation (Fig. 3D). In the absence of irradiation, Gel@L-Arg (0.5 %) showed effects similar to the AGA group. However, under 660 nm laser irradiation, NO produced by Gel@L-Arg (0.5 % + NIR) and Gel@L-Arg (1 % + NIR) significantly promoted HUVECs proliferation. Notably, Gel@L-Arg (0.5 % + NIR), generating a lower NO concentration, had the most pronounced effect on HUVECs viability, indicating that low-concentration NO has a reparative effect on DHT-induced HUVECs damage. As shown in Fig. 3B, E, cell migration results indicated that DHT reduced HUVECs migration in the AGA group, achieving only 19.55 ± 1.24 % migration rate compared to the Control. Consistent with the cell viability findings, NO generated under 660 nm irradiation enhanced cell migration, with the most significant improvement observed in the Gel@L-Arg (0.5 % + NIR) group, reaching 97.55 ± 0.1 %. This result reinforces the advantageous role of low-concentration NO in enhancing cell activity and demonstrates its potential in vascular repair. Subsequently, an angiogenesis assay was conducted. As shown in Fig. 3C, F, under 660 nm laser irradiation, the total vascular length in the Gel@L-Arg (0.5 % + NIR) group significantly increased compared to other groups, confirming that low-concentration NO effectively promotes angiogenesis, thereby validating the hypothesis. These experiments suggest that low-concentration NO generated by Gel@L-Arg (0.5 % + NIR) under NIR irradiation promotes angiogenesis *in vitro*. This enhancement in vascular growth may benefit AGA patients by repairing degenerated blood vessels, regulating follicular microcirculation.

3.4. NO promotes hair growth by repairing damaged human dermal papilla cells (HDPCs)

In hair follicles, androgen receptors are predominantly expressed by HDPCs, and sustained local stimulation of HDPCs by DHT leads to functional deterioration, resulting in reduced hair growth, accelerated transition from the anagen to telogen phase [31]. This study investigates the effects of Gel@L-Arg on HDPCs in detail. As shown in Fig. 4C, cell viability assays demonstrated that NO generated by 660 nm laser irradiation of Gel@L-Arg (0.5 % + NIR) and Gel@L-Arg (1 % + NIR) increased HDPCs proliferation rates in DHT-damaged groups, 131.6 ± 4.6 % and 112.2 ± 1.6 %, respectively. Indicating that NO also has a reparative effect on DHT-induced HDPCs damage, providing robust evidence for the treatment of AGA. The cell migration assay, as shown in Fig. 4B and **Fig. S2**, DHT reduced HDPCs migration rates whereas NO generated under 660 nm laser irradiation significantly enhanced HDPCs migration (88.3 ± 1.7 %). The scratch area in HDPCs treated with low-concentration NO for 24 h reduced more markedly than in the AGA and Control groups, demonstrating the potential of low-concentration NO in repairing damaged HDPCs and suggesting its potential for *in vivo* treatment of AGA. Previous studies have shown that DHT can induce HDPCs in AGA patients' hair follicles to release IL-6, triggering an inflammatory response that inhibits hair follicle growth [32]. qRT-PCR results in Fig. 4D reveal that NO treatment markedly reduced IL-6 secretion by HDPCs, with levels in Gel@L-Arg (0.5 % + NIR) and Gel@L-Arg (1 % + NIR) groups approaching those of the Control group. The lowest IL-6 levels were observed in the Gel@L-Arg (0.5 % + NIR) group, suggesting that low-concentration NO can mitigate androgen-induced inflammation and subsequently promote hair growth. Exogenous MMP-9 has been shown to promote endothelial cell growth and angiogenesis [33]. As illustrated in Fig. 4E, qRT-PCR analysis demonstrated that low-concentration NO treatment increased MMP-9 secretion by HDPCs, which may aid in the formation of blood vessels around hair follicles, improve circulation, and promote hair growth. These

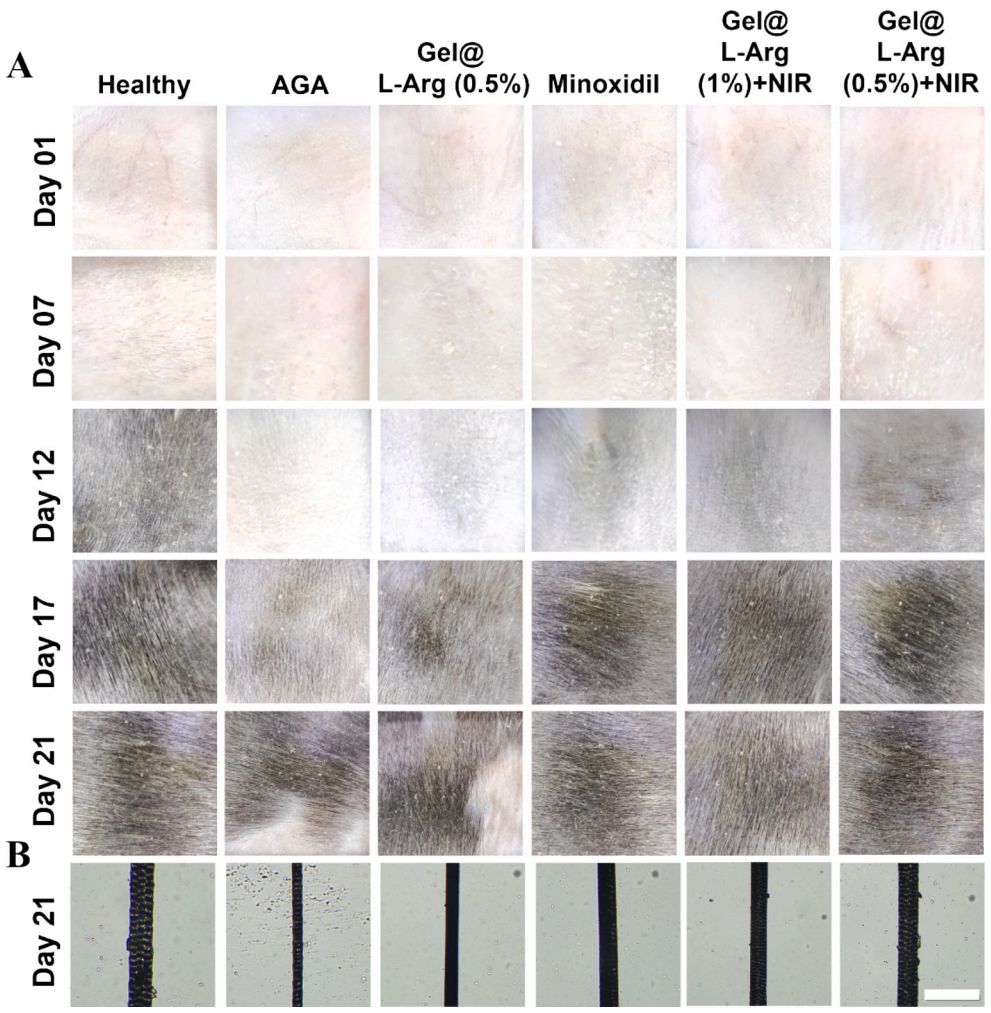

Fig. 6. Evaluation of hair regeneration. (A) Dermoscopic images over the 21-day period. (B) Microscopic images of newly regenerated hair in each group on day 21.

experiments indicate that NO, as a crucial signaling molecule mediating various pathways, can participate in hair follicle development and effectively repair damaged follicles by modulating the expression of mRNA factors. Additionally, the concentration of NO influence hair follicle growth and development, with low concentrations being more favorable for follicle regeneration.

3.5. Evaluation of hair regeneration effects

An AGA model was established in C57BL/6 mice following previous reports. Female mice were selected to eliminate endogenous androgen influences, and AGA was induced by daily injections of dihydrotestosterone (DHT). As shown in Fig. 5B, photographs of each group were taken on days 1, 7, 12, 17, and 21 to monitor dorsal hair growth. By day 12, the dorsal region of the NO-treated group with NIR irradiation had turned visibly gray, contrasting noticeably with the AGA, Gel@L-Arg (0.5 %), and Minoxidil groups approaching the coloration of the Healthy group (Fig. S3B). This observation directly demonstrates the efficacy of NO in treating AGA, with prominent results. Skin dermoscopy further revealed that the treatment effect persisted until the end of the experiment (Fig. 6A), and regenerated hair in the NO-treated group was comparable to the Healthy group in terms of both coverage area (Fig. S3D) and weight, with low-concentration NO showing particularly notable results (Fig. 5C, D). As shown in Fig. 6B, microscopic images of regenerated hair demonstrated that newly grown hair in the AGA group was thinner and showed less scale, whereas the low-concentration NO group displayed thicker hair shafts with intact scales, comparable to the Healthy group, confirming the successful establishment of the AGA model and its clinical relevance. During the experiment, all mice exhibited an increase in body weight (Fig. S3C), indicating that hormone injections did not interfere with normal physiological activities, lending further validity to the experimental process.

Further evaluation through HE staining of skin tissue sections (Fig. 7A) showed a significant reduction in follicle count in the AGA group, with an increase in the number of telogen and catagen follicles, as well as follicle shrinkage. In contrast, the Gel@L-Arg (0.5 % + NIR) group exhibited a higher follicle count with intact structure, similar to the Healthy group after treatment, indicating that low-concentration NO promotes follicle regeneration. CD31, a marker for vascular endothelial cells, reflects the distribution of blood vessels within the tissue. Based on CD31 immunohistochemical staining of skin tissue (Fig. 7B), the Gel@L-Arg (0.5 % + NIR) group displayed the highest positive CD31 expression, closely resembling that of the Healthy group. Quantitative comparison (Fig. S4B) confirmed that low-concentration NO significantly enhances angiogenesis [34]. Ki67, a marker of cell proliferation, is primarily expressed in the nucleus. Low-concentration NO notably increased cell viability, further promoting hair growth (Fig. 7B) [35]. To assess the impact of NO on skin tissue, 3-nitrotyrosine staining was performed as it is widely regarded as an indicator of NO production [36]. As illustrated in Fig. 7B, NO levels were highest in the Gel@L-Arg (1 % + NIR) group, with the Gel@L-Arg (0.5 % + NIR) group producing more NO than the AGA, Gel@Arg (0.5 %), and Minoxidil groups. This demonstrates the capability of Gel@L-Arg to achieve controlled NO release by encapsulating different concentrations of L-Arg, thereby

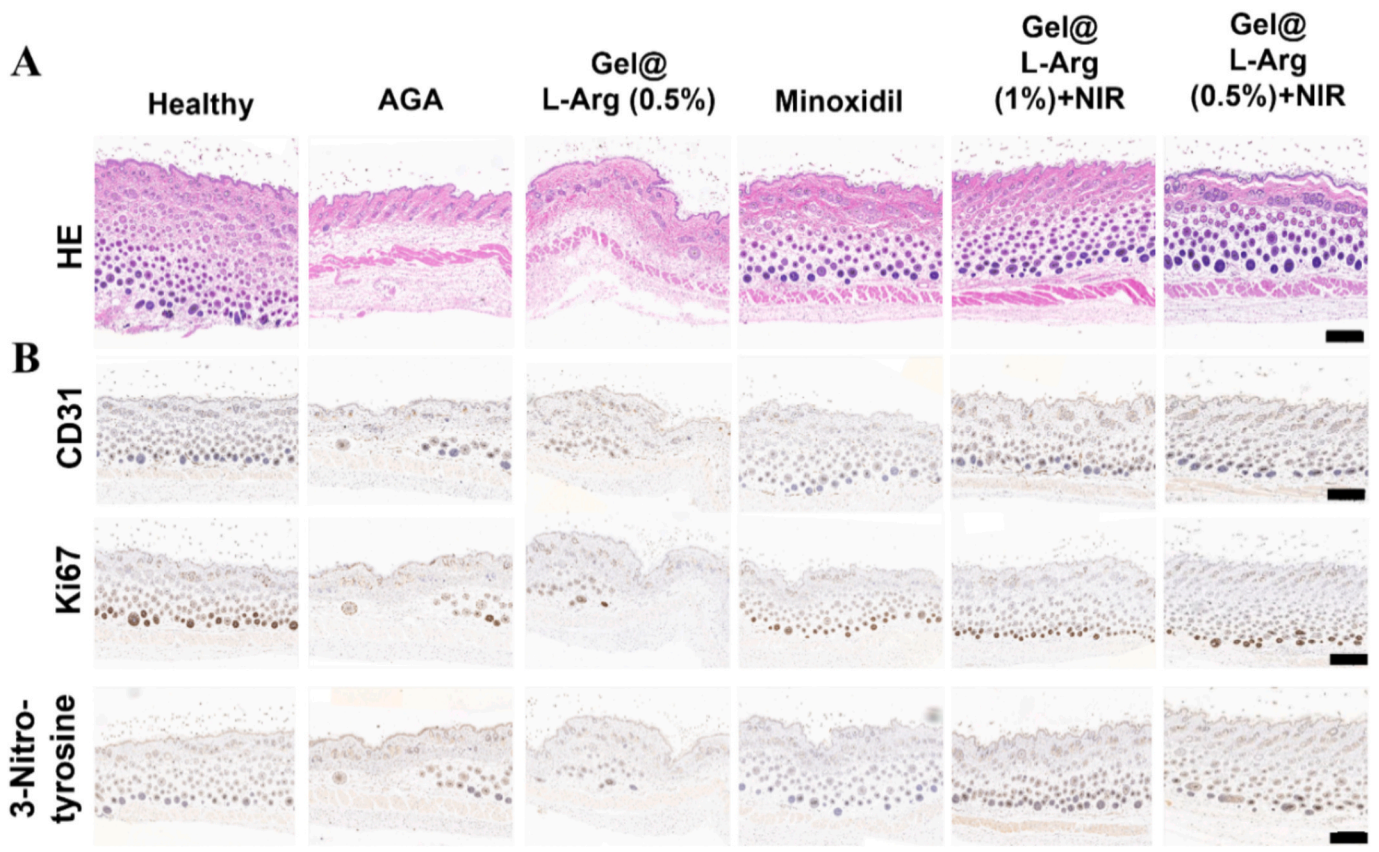

Fig. 7. Histological evaluation of mouse skin tissue. (A) HE-stained images of dorsal skin from mice, scale bar = 200 μm. (B) Immunohistochemical staining for CD31, Ki67, and 3-nitrotyrosine, scale bar = 200 μm.

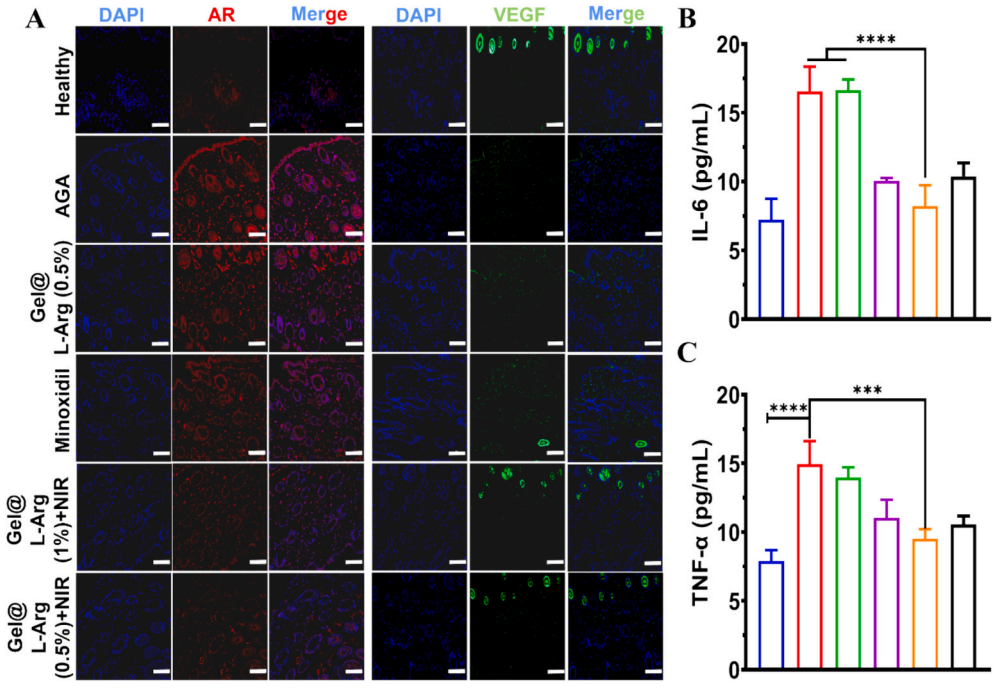

Fig. 8. Regulation of skin tissue microenvironment. (A) Fluorescence expression of AR and VEGF in skin tissue across groups, scale bar = 100 μm. (B) IL-6 levels in mouse skin across groups ($n = 4$). (C) TNF-α levels in mouse skin across groups (n = 4). *$P < 0.05$; **$P < 0.01$; ***$P < 0.001$; ****$P < 0.0001$.

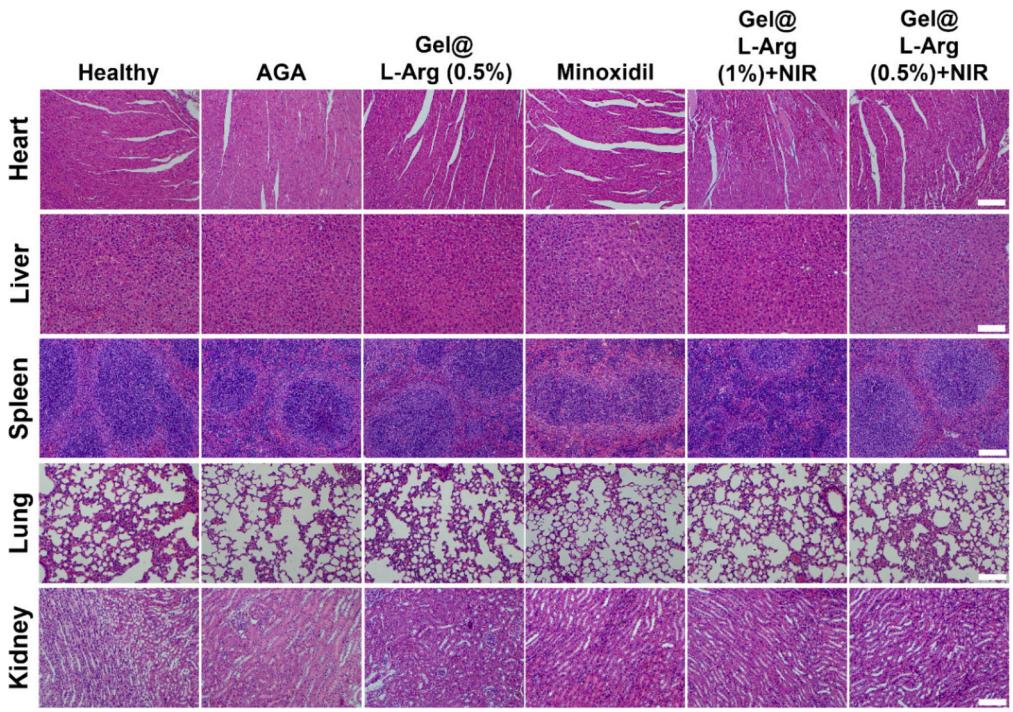

Fig. 9. H&E staining pictures of major organs in mice, scale bar = 250 μm.

meeting varying therapeutic needs.

3.6. Regulation of skin tissue microenvironment

To elucidate the effect of NO on the microenvironment surrounding hair follicles, relevant indicators in skin tissue were assessed. Studies have shown that IL-6 and TNF-α are released around hair follicles in AGA patients, promoting follicular cell apoptosis and inhibiting hair growth [37]. Therefore, after 21 days of treatment, the dorsal skin tissue of mice was homogenized, and the supernatant was collected to measure TNF-α and IL-6 levels. As shown in Fig. 8B, C, IL-6 (16.56 ± 1.85 %) and TNF-α (14.94 ± 1.7 %) levels in the AGA group were higher than those in the treatment groups, with the lowest levels observed in the Gel@L-Arg (0.5 % + NIR) group, closely resembling the Healthy group. This indicates that low-concentration NO reduces IL-6 (8.23 ± 1.5 %) and TNF-α (9.51 ± 0.7 %) expression, exhibiting anti-inflammatory effects. As shown in Fig. 8A and Fig. S5A, immunofluorescence staining was used to assess AR protein expression in mice treated with various materials. Immunofluorescence of skin sections showed deeper AR protein staining in the AGA group, indicating increased expression due to competitive AR binding induced by subcutaneous injection of DHT suspension, which elevated AR expression around hair follicles [38]. Only a small area around hair follicles in the Healthy group displayed staining, suggesting limited AR protein expression around normal follicles. In contrast, the treatment groups showed reduced AR expression around follicles, with the Gel@L-Arg (0.5 % + NIR) group exhibiting the lowest AR levels, closely approximating the healthy group, suggesting that low-concentration NO suppresses AR expression, thereby promoting follicular regeneration. Vascular endothelial growth factor (VEGF) is a key growth factor with pro-angiogenic activity that promotes endothelial cell mitosis and anti-apoptosis, increases vascular permeability, and facilitates cell migration, which is essential for vascular regulation [39]. As shown in Fig. 8A and Fig. S5B, VEGF expression in the AGA group was significantly lower, whereas the treatment groups exhibited generally higher VEGF levels, with the low-concentration NO treatment group displaying VEGF expression most comparable to the Healthy group. The Gel@L-Arg effectively inhibits inflammatory responses in hair follicles, promotes vascularization to repair damaged follicles, and improves the hair growth microenvironment, demonstrating high efficacy in treating AGA.

3.7. Biocompatibility assessment

HE staining of the major organs from each group of mice showed no observable tissue damage or toxicity (Fig. 9). Additionally, as shown in Fig. S6, biochemical analysis of serum biomarkers after treatment revealed that, compared to the Healthy group, all indicators, including liver function and kidney function, met the standard requirements. These findings suggest that Gel@L-Arg possesses good biosafety and has potential for practical clinical application.

3.8. Prospects for the treatment of AGA

Androgenetic alopecia (AGA) is a common clinical condition that causes significant distress to individuals. In recent years, various treatment strategies have emerged, including minoxidil, finasteride, platelet-rich plasma, low-level laser therapy (LLLT), and hair transplantation [40]. In this study, by integrating light-controlled release technology, hydrogel, and the potential of NO in treating AGA, we addressed a series of issues such as the difficulty in controlling NO release and adjusting its concentration. We developed a NIR light-controlled NO delivery system (Gel@L-Arg), which achieved promising results in the treatment of AGA. With advancements in treatment technologies, we have observed that compared to single-treatment approaches, combination therapies hold great promise in the management of AGA. Inspired by laser therapy and pharmacological treatments, we made corresponding improvements in this study and boldly speculate that future treatment options for AGA should consider integrated and personalized approaches. We are hopeful about the prospects of AGA treatment and plan to recruit volunteers for clinical trials to observe the effects. By combining optimal treatment strategies, we aim to provide patients with the best treatment outcomes at a low cost to address their hair loss concerns.

4. Conclusions

In this study, the construction of Gel@L-Arg successfully achieved controlled NO release with adjustable concentration, demonstrating efficacy in treating androgenetic alopecia (AGA). Serving as a transdermal delivery carrier, this system exhibited structural and temperature stability. Under near-infrared (NIR) light irradiation, ROS generated by Ce6 rapidly oxidized L-Arg, leading to the immediate and controlled release of NO, overcoming the limitation of its short half-life. After 5 min of irradiation, the NO concentration in Gel@L-Arg (1 %) was >1.5 times that in Gel@L-Arg (0.5 %), achieving on-demand release of NO. In *in vitro* cell experiments, NO generated by irradiating Gel@L-Arg (0.5 %) effectively promoted angiogenesis, with its vascular formation ability exceeding that of the model group by more than threefold. It also significantly enhanced HDPCs viability (131.6 ± 4.6 %) and migration ability (88.3 ± 1.7 %). This approach shows promise for treating AGA by improving hair follicle vitality, promoting vascular repair, and inhibiting inflammatory responses. *In vitro* cell experiments identified the optimal NO concentration for treatment, showing promise in enhancing follicle vitality, promoting vascular repair, and inhibiting inflammatory responses for AGA treatment. *In vivo* animal studies further revealed that this hydrogel could reduce IL-6 and TNF-α expression to counter inflammation, upregulate VEGF and CD31 expression to improve follicular nutrient supply, and regulate androgen levels and proliferative proteins to enhance the follicular microenvironment, demonstrating effective clinical treatment outcomes and biosafety. Thus, this study provides a novel approach for gas-mediated treatment of AGA through controlled NO release, offering valuable insight into controlled gas release therapies for other diseases.

CRediT authorship contribution statement

Hui Xing: Writing – original draft, Investigation, Formal analysis, Data curation. **Yucheng Wang:** Writing – original draft, Investigation, Formal analysis, Data curation. **Shengling Huang:** Writing – original draft, Resources, Formal analysis, Data curation. **Huanqi Peng:** Writing – original draft, Formal analysis, Data curation. **Ziyi Zhao:** Investigation, Formal analysis, Data curation. **Yuhui Yang:** Resources, Formal analysis, Data curation. **Xiaoxu Zhu:** Writing – original draft, Resources, Funding acquisition, Data curation. **Guowei Li:** Writing – original draft, Funding acquisition, Formal analysis, Data curation. **Dong Ma:** Writing – original draft, Funding acquisition, Formal analysis, Data curation.

Authors contributions

H.X., Y.W. and S.H. contributed equally to this work. H.X., X.Z., G.L. and D.M. designed the work. H.X. and Y.W. wrote the manuscript. H.X., Y.W. and S.H. performed the experiments and collected the data. H.P., Z. Z. and Y.Y. helped with some measurements. X.Z., H.X. and Y.W. analyzed the data. D.M. and G.L. provided research funding. All authors have given approval to the final version of the manuscript.

Declaration of competing interest

The authors declare that they have no known competing financial interests or personal relationships that could have appeared to influence the work reported in this paper.

Acknowledgments

This work was financially supported by the National Natural Science Foundation of China (32171369 and 82102113), the Science and Technology Program of Guangzhou (2024A04J3478) and the Fundamental Research Funds for the Central Universities (11623410).

Appendix A. Supplementary data

Supplementary data to this article can be found online at https://doi.org/10.1016/j.ijbiomac.2025.140751.

Data availability

Data will be made available on request.

References

[1] S. Gupta, I. Goyal, A. Mahendra, Quality of life assessment in patients with androgenetic alopecia, Int. J. Trichology 11 (4) (2019) 147–152.
[2] V. Soni, Androgenic alopecia: a counterproductive outcome of the anabolic effect of androgens, Med. Hypotheses 73 (3) (2009) 420–426.
[3] W. Cranwell, R. Sinclair, Male androgenetic alopecia, (2015).
[4] W. Hu, S. Shi, Y. Xu, Y. Zhang, J. Hu, Q. Bian, X. Ma, Y. Ye, S. Yang, X. Sheng, Platinum Nanozyme-loaded dissolving microneedles scavenge ROS and Promote lineage progression for androgenetic alopecia treatment, small, Methods (2024) 2401176.
[5] Z. Chen, H. Zhang, Y. Lyu, K. Lv, H. Xing, P. Shen, Z. Guo, G. Li, D. Ma, Octopus-inspired adaptive molecular motion for synergistic Photothermal and nitric oxide antibacterial therapy in diabetic wound repair, Adv. Funct. Mater. 2402591 (2024).
[6] H. Xing, H. Peng, Y. Yang, K. Lv, S. Zhou, X. Pan, J. Wang, Y. Hu, G. Li, D. Ma, Nitric oxide synergizes minoxidil delivered by transdermal hyaluronic acid liposomes for multimodal androgenetic-alopecia therapy, Bioact. Mater. 32 (2024) 190–205.
[7] T. Yang, A.N. Zelikin, R. Chandrawati, Progress and promise of nitric oxide-releasing platforms, Adv. Sci. 5 (6) (2018) 1701043.
[8] L.B. Vong, Y. Nagasaki, Nitric oxide nano-delivery systems for cancer therapeutics: advances and challenges, Antioxidants 9 (9) (2020) 791.
[9] H. Ma, T. Wang, G. Li, J. Liang, J. Zhang, Y. Liu, W. Zhong, P. Li, A photo-modulated nitric oxide delivering hydrogel for the accelerated healing of biofilm infected chronic wounds, Acta Biomater. 188 (2024) 169–183.
[10] Z. Chen, H. Zhang, Y. Lyu, K. Lv, H. Xing, P. Shen, Z. Guo, G. Li, D. Ma, Octopus-inspired adaptive molecular motion for synergistic Photothermal and nitric oxide antibacterial therapy in diabetic wound repair, Adv. Funct. Mater. 34 (41) (2024) 2402591.
[11] A. Ahsan, W.-X. Tian, M.A. Farooq, D.H. Khan, An overview of hydrogels and their role in transdermal drug delivery, international journal of polymeric materials and polymeric, Biomaterials 70 (8) (2021) 574–584.
[12] Y. Zheng, A. Baidya, N. Annabi, Molecular design of an ultra-strong tissue adhesive hydrogel with tunable multifunctionality, Bioact. Mater. 29 (2023) 214–229.
[13] H. Guo, S. Huang, A. Xu, W. Xue, Injectable adhesive self-healing multiple-dynamic-bond crosslinked hydrogel with photothermal antibacterial activity for infected wound healing, Chem. Mater. 34 (6) (2022) 2655–2671.
[14] Y. Yuan, S. Shen, D. Fan, A physicochemical double cross-linked multifunctional hydrogel for dynamic burn wound healing: shape adaptability, injectable self-healing property and enhanced adhesion, Biomaterials 276 (2021) 120838.
[15] L. Yuwen, Q. Qiu, W. Xiu, K. Yang, Y. Li, H. Xiao, W. Yang, D. Yang, L. Wang, Hyaluronidase-responsive phototheranostic nanoagents for fluorescence imaging and photothermal/photodynamic therapy of methicillin-resistant Staphylococcus aureus infections, Biomater. Sci. 9 (12) (2021) 4484–4495.
[16] S. Wang, S. Tavakoli, R.P. Parvathaneni, G.N. Nawale, O.P. Oommen, J. Hilborn, O. P. Varghese, Dynamic covalent crosslinked hyaluronic acid hydrogels and nanomaterials for biomedical applications, Biomater. Sci. 10 (22) (2022) 6399–6412.
[17] Z.-H. Xie, C.-S. He, D.-N. Pei, Y. Dong, S.-R. Yang, Z. Xiong, P. Zhou, Z.-C. Pan, G. Yao, B. Lai, Review of characteristics, generation pathways and detection methods of singlet oxygen generated in advanced oxidation processes (AOPs), Chem. Eng. J. 468 (2023) 143778.
[18] G. Li, K. Lv, Q. Cheng, H. Xing, W. Xue, W. Zhang, Q. Lin, D. Ma, Enhanced bacterial-infected wound healing by nitric oxide-releasing topological supramolecular nanocarriers with self-optimized cooperative multi-point anchoring, Adv. Sci. 10 (11) (2023) 2206959.
[19] C. Hu, F. Zhang, L. Long, Q. Kong, R. Luo, Y. Wang, Dual-responsive injectable hydrogels encapsulating drug-loaded micelles for on-demand antimicrobial activity and accelerated wound healing, J. Control. Release 324 (2020) 204–217.
[20] S. Bhattacharya, A. Ghosh, S. Maiti, M. Ahir, G.H. Debnath, P. Gupta, M. Bhattacharjee, S. Ghosh, S. Chattopadhyay, P. Mukherjee, Delivery of thymoquinone through hyaluronic acid-decorated mixed Pluronic® nanoparticles to attenuate angiogenesis and metastasis of triple-negative breast cancer, J. Control. Release 322 (2020) 357–374.
[21] Z. Zhang, W. Li, D. Chang, Z. Wei, E. Wang, J. Yu, Y. Xu, Y. Que, Y. Chen, C. Fan, A combination therapy for androgenic alopecia based on quercetin and zinc/copper dual-doped mesoporous silica nanocomposite microneedle patch, Bioact. mater. 24 (2023) 81–95.
[22] Y.-W. Ding, Y. Li, Z.-W. Zhang, J.-W. Dao, D.-X. Wei, Hydrogel forming microneedles loaded with VEGF and Ritlecitinib/polyhydroxyalkanoates nanoparticles for mini-invasive androgenetic alopecia treatment, Bioact. Mater. 38 (2024) 95–108.

[23] Y. Kim, Y.C. Ryu, H.S. Min, H. Yang, J. Nam, C. Lee, D.J. Um, M. Kim, P. Atzei, R.d. B. Francisco, Dual-mode vasodilator M119 delivery to hair follicle via dissolving microneedle for advanced alopecia treatment, Adv. Therap. 5 (8) (2022) 2200052.
[24] L. Liang, T. Liu, Q. Ouyang, S. Li, C. Li, Solid phase synthesis of oxidized sodium alginate-tobramycin conjugate and its application for infected wound healing, Carbohydr. Polym. 295 (2022) 119843.
[25] L. Li, X. Wu, J. Wu, X. Zhang, F. Miao, J. Wang, J. Lu, J. Liu, Z. Chen, Z. Tai, Transdermal delivery of Fn14 siRNA using a novel composite ionic liquid for treatment of psoriasis-like skin lesions, J. Control. Release 365 (2024) 818–832.
[26] C. Li, X. Luo, L. Li, Y. Cai, X. Kang, P. Li, Carboxymethyl chitosan-based electrospun nanofibers with high citral-loading for potential anti-infection wound dressings, Int. J. Biol. Macromol. 209 (2022) 344–355.
[27] H. Guo, S. Huang, X. Yang, J. Wu, T.B. Kirk, J. Xu, A. Xu, W. Xue, Injectable and self-healing hydrogels with double-dynamic bond tunable mechanical, gel–sol transition and drug delivery properties for promoting periodontium regeneration in periodontitis, ACS Appl. Mater. Interfaces 13 (51) (2021) 61638–61652.
[28] T. Cui, Y. Wu, C. Ni, Y. Sun, J. Cheng, Rheology and texture analysis of gelatin/dialdehyde starch hydrogel carriers for curcumin controlled release, Carbohydr. Polym. 283 (2022) 119154.
[29] X. Yang, X. Shi, Y. Zhang, J. Xu, J. Ji, L. Ye, F. Yi, G. Zhai, Photo-triggered self-destructive ROS-responsive nanoparticles of high paclitaxel/chlorin e6 co-loading capacity for synergetic chemo-photodynamic therapy, J. Control. Release 323 (2020) 333–349.
[30] Z. Deng, M. Chen, F. Liu, Y. Wang, S. Xu, K. Sha, Q. Peng, Z. Wu, W. Xiao, T. Liu, Androgen receptor–mediated paracrine signaling induces regression of blood vessels in the dermal papilla in androgenetic alopecia, J. Invest. Dermatol. 142 (8) (2022) 2088–2099 (e9).
[31] Y. Shimizu, E.H. Ntege, H. Sunami, Y. Inoue, Regenerative medicine strategies for hair growth and regeneration: a narrative review of literature, Regen. ther. 21 (2022) 527–539.
[32] M.H. Kwack, J.S. Ahn, M.K. Kim, J.C. Kim, Y.K. Sung, Dihydrotestosterone-inducible IL-6 inhibits elongation of human hair shafts by suppressing matrix cell proliferation and promotes regression of hair follicles in mice, J. Invest. Dermatol. 132 (1) (2012) 43–49.
[33] A. Pozzi, W.F. LeVine, H.A. Gardner, Low plasma levels of matrix metalloproteinase 9 permit increased tumor angiogenesis, Oncogene 21 (2) (2002) 272–281.
[34] C.C. Figueiredo, N. Braga Pereira, L.X. Pereira, L.A. Machado Oliveira, P. Peixoto Campos, S. Passos Andrade, L. Moro, Double Immunofluorescence Labeling for CD31 and CD105 as a Marker for Polyether Polyurethane-Induced Angiogenesis in Mice, 2019.
[35] G. Tong, G. Zhang, J. Liu, Z. Zheng, Y. Chen, P. Niu, X. Xu, Cutoff of 25% for Ki67 expression is a good classification tool for prognosis in colorectal cancer in the AJCC-8 stratification, Oncol. Rep. 43 (4) (2020) 1187–1198.
[36] H. Ahsan, 3-Nitrotyrosine: a biomarker of nitrogen free radical species modified proteins in systemic autoimmunogenic conditions, Hum. Immunol. 74 (10) (2013) 1392–1399.
[37] R. Rückert, G. Lindner, S. Bulfone-Paus, R. Paus, High-dose proinflammatory cytokines induce apoptosis of hair bulb keratinocytes in vivo, Br. J. Dermatol. 143 (5) (2000) 1036–1039.
[38] D. Fu, J. Huang, K. Li, Y. Chen, Y. He, Y. Sun, Y. Guo, L. Du, Q. Qu, Y. Miao, Dihydrotestosterone-induced hair regrowth inhibition by activating androgen receptor in C57BL6 mice simulates androgenetic alopecia, Biomed. Pharmacother. 137 (2021) 111247.
[39] C.S. Melincovici, A.B. Boşca, S. Şuşman, M. Mărginean, C. Mihu, M. Istrate, I.-M. Moldovan, A.L. Roman, C.M. Mihu, Vascular endothelial growth factor (VEGF)-key factor in normal and pathological angiogenesis, Romanian J. Morphol. Embryol. 59 (2) (2018) 455–467.
[40] M.J. Nagata, N. De Campos, M.R. Messora, N.M. Pola, C.S. Santinoni, S.R. Bomfim, S.E. Fucini, E. Ervolino, J.M. De Almeida, L.H. Theodoro, Platelet-rich plasma, low-level laser therapy, or their combination promotes periodontal regeneration in fenestration defects: a preliminary in vivo study, J. Periodontol. 85 (6) (2014) 770–778.